Biomaterials 279 (2021) 121207

Contents lists available at ScienceDirect

Biomaterials

journal homepage: www.elsevier.com/locate/biomaterials

Construction of functional biliary epithelial branched networks with predefined geometry using digital light stereolithography

Elsa Mazari-Arrighi [a,b,c], Dmitry Ayollo [a,b,c], Wissam Farhat [a,b,c], Auriane Marret [a,b,c], Emilie Gontran [d,e], Pascale Dupuis-Williams [e,f], Jerome Larghero [a,b], Francois Chatelain [a,b,c], Alexandra Fuchs [a,b,c,*]

[a] Université de Paris, Inserm, U976 HIPI, F-75006, Paris, France
[b] AP-HP, Hôpital Saint-Louis, 1 avenue Vellefaux, F-75010, Paris, France
[c] CEA, IRIG, F-38000, Grenoble, France
[d] INSERM U-1279, Gustave Roussy, Villejuif, F-94805, France
[e] Université Paris-Saclay, Inserm, Physiopathogenèse et traitement des maladies du foie, F-94800, Villejuif, France
[f] ESPCI Paris, Université PSL, F-75005, Paris, France

ARTICLE INFO

Keywords:
Tissue engineering
Bile ducts
Biliary tree
3D bioprinting
DLP stereolithography
Cholangiocytes

ABSTRACT

Cholangiocytes, biliary epithelial cells, are known to spontaneously self-organize into spherical cysts with a central lumen. In this work, we explore a promising biocompatible stereolithographic approach to encapsulate cholangiocytes into geometrically controlled 3D hydrogel structures to guide them towards the formation of branched tubular networks. We demonstrate that within the appropriate mix of hydrogels, normal rat cholangiocytes can proliferate, migrate, and organize into branched tubular structures with walls consisting of a cell monolayer, transport fluorescent dyes into the luminal space, and show markers of epithelial maturation such as primary cilia and continuous tight junctions. The resulting structures have dimensions typically found in the intralobular and intrahepatic biliary tree and are stable for weeks, without any requirement of bulk supporting material, thereby offering total access to the external side of these biliary epithelial constructs.

1. Introduction

Liver tissue engineering is an actively developing research area in the field of drug screening to develop more physiologically relevant toxicity assays and models of liver diseases. Furthermore, it is a promising solution for regenerative medicine to alleviate the need for donor liver tissue. In recent years, significant progress has been made in culturing primary or iPSC-derived hepatocytes in the form of spheroids or organoids to achieve higher differentiation and maintain better functionality *in vitro* [1–6]. To date, the most advanced example of this approach was described by Takebe et al., who managed to produce liver buds composed of iPS-derived endoderm, endothelial and mesenchymal cells grown to form organoids that were shown to rescue hepatic functions in a mouse model of acute liver failure [7]. Such an approach has the potential to create relevant models of metabolic liver diseases, as well as to ultimately treat the partial failure of liver functions. However, they do not take into account the critical role played by the bile ducts and ductule network in collecting and clearing toxic compounds and metabolites from the hepatic tissue.

The human biliary tree consists of the intrahepatic and extrahepatic sections. The intrahepatic biliary tree is composed of ductules that collect and modify the bile from the bile canaliculi formed by hepatocytes in the liver lobules. The intrahepatic ductules gradually merge into the common hepatic duct which leads to the extrahepatic biliary tree [8,9]. Over the past few years, there have been a few successful attempts to produce bio-artificial bile ducts (BABD). For example, in 2019, Tysoe et al. have described a way to build a bile duct with a lumen diameter of 250 μm using a rolled polyglycolic acid or a collagen hydrogel layer as a scaffold for cholangiocytes isolated from murine liver and amplified as organoids [10]. Another approach was described by Chen et al., in 2018 in which authors used cholangiocyte-like cells from the murine liver to seed the outer surface of polyethersulfone hollow fiber membranes functionalized with L-Dopa and collagen [11]. The result was a BABD with an inside-out inverted polarity and a diameter of 1 mm. While the

* Corresponding author. Inserm U976, porte 15B, Hôpital Saint- Louis, 1 Avenue Claude Vellefaux, Paris, 75010, France.
E-mail address: alexandra.fuchs@cea.fr (A. Fuchs).

https://doi.org/10.1016/j.biomaterials.2021.121207
Received 12 April 2021; Received in revised form 11 October 2021; Accepted 20 October 2021
Available online 28 October 2021

above-mentioned works mark obvious progress in extrahepatic bile duct reconstruction, reproduction of the intrahepatic part of the biliary tree is more challenging due to both its size and its complexity. Indeed, the intrahepatic biliary tree permeates every level of liver anatomy from the hepatic hilum to the liver lobule, with internal luminal diameters ranging from 800 μm in the interlobular ducts down to 10 μm inside the lobules.

Using the relatively popular top-down approach of decellularization and subsequent recellularization of the whole organ, the liver vasculature has been successfully repopulated with endothelial cells [12]. However, the recellularization approach for the biliary tree showed limited success [13]. This may be due to several factors ranging from the intricate biology of cholangiocytes to the tortuous and complex architecture of the intrahepatic biliary tree.

Bottom-up approaches to *de novo* engineering of the intrahepatic biliary tree have been pursued using hydrogel matrices. *In vitro,* extracellular matrix (ECM) substitutes such as type 1 collagen or Matrigel (an ECM hydrogel produced by the mouse Engelbreth-Holm-Swarm sarcoma cell line) have shown promising results both for cholangiocytes alone or in co-culture with hepatocytes [14,15]. Cholangiocytes, known to have a certain degree of *in vitro* morphogenic capability, spontaneously form cysts when cultured in natural or synthetic hydrogels [11,16] and cystic organoids obtained from primary cholangiocytes have been shown to repair intrahepatic bile ducts when transplanted in a human liver undergoing *ex vivo* normothermic perfusion [17]. However, elongated duct formation *in vitro* in Matrigel or type 1 collagen is rarely seen [18–24]. Another drawback is the lack of control over the direction, length, branching, and diameter of occasionally forming tubular structures.

A promising approach to building tissue constructs with controlled geometry is 3D bioprinting. In this field, Lutolf's team illustrated how extrusion-printing of a high-density suspension of gut epithelial cells in a Matrigel/collagen hydrogel could lead to self-organization of cells into tubes with a luminal diameter of 100–200 μm [25]. To reach an even higher resolution, in particular, to reach features in the range of 10–100 μm, digital light processing (DLP) stereolithography is particularly efficient. This approach was illustrated in a publication by Ma et al., where different types of cells (iPS-derived hepatic progenitor cells, endothelial cells, and adipose-derived stem cells) were encapsulated in imbricated 3D structures mimicking the hexagonal design of the liver lobule [26]. The resulting construct exhibited enhanced hepatic phenotypes and metabolite activity. However, the reconstruction of the biliary network was not addressed in their work.

In our study, we used normal rat cholangiocytes (NRC) and DLP stereolithography to produce Biliary Structures by PhotoPolymerization (BSPPs) with controlled geometry. After several days of culture, the self-organization of branched tubular structures guided by the predefined geometry of the hydrogel scaffold leads to the formation of BSPPs. These tubes spanning hundreds of microns had a central closed lumen with walls composed of a monolayer of cells with an epithelium phenotype, including the presence of tight junctions and primary cilia facing the lumen. Our results also demonstrate that these cholangiocyte structures possess functional transport properties of bile ducts.

2. Material and methods

2.1. Culture of cholangiocytes in 2D

NRC, a cholangiocyte cell line developed by Vroman and LaRusso [27] were maintained on collagen-coated culture vessels in Dulbecco's modified eagle medium F12 (DMEM F12, Gibco), non-essential amino acids (Gibco), lipid concentrate (Gibco), vitamin solution (Gibco), L-glutamine (Gibco), soybean trypsin inhibitor (Sigma), dexamethasone (Sigma), ethanolamine (Sigma), bovine pituitary extract (Gibco), Triiodo-L-thyronine (Sigma), Insulin-transferrin-Selenium (Gibco), and penicillin-streptomycin (Gibco) supplemented with 5% fetal bovine serum as described by De Groen et al. [28].

NRCs from passages 3–12 were used for the 3D stereolithography experiments.

2.2. Fabrication of BSPP using DLP stereolithography

Before 3D stereolithography, photopolymerizable hydrogels were prepared with 0.2% (w/v) type I methacrylated collagen (C^{MA}, Advanced BioMatrix), 0.3% (w/v) methacrylated hyaluronic acid (HA^{MA}, Advanced BioMatrix), 0.14% (w/v) fibrinogen (FG, Sigma), and 1% (w/v) lithium phenyl-2,4,6 trimethyl-benzoyl phosphinate (LAP, Allevi). NRC were harvested with 0.25% trypsin-EDTA (Sigma) and diluted to cell concentrations of 10^7 NRC/mL in photopolymerizable hydrogel.

The 3D stereolithography experiments were performed using an Olympus IX83-inverted microscope (Olympus Corporation) equipped with a DMD-based UV patterned illumination device (PRIMO, Alveole). The wavelength of the laser is 375 nm. Rasterized image files are sent to the DMD device which is an array of approximately two million micromirrors that can be controlled individually to generate the optical pattern. The optical photopattern is then projected through a microscope lens onto the photopolymerizable hydrogel containing NRCs.

Photopolymerizable hydrogels containing 10^7 NRCs/mL were dispensed by 30 μL with a pipette into the space between a methacrylated glass coverslip and a polydimethylsiloxane (PDMS) stamp. The whole device was then loaded to the microscope slide holder and exposed to the UV pattern through a 10x at 20 mJ/mm^2 dose. After UV exposure, the PDMS stamp was peeled off and the unpolymerized part of photopolymerizable hydrogel containing NRC was removed and washed off with PBS buffer (Sigma).

2.3. Culture of BSPPs

After 3D stereolithography, the BSPPs were transferred to a petridish or a well plate and cultured in NRC culture medium. For the Matrigel-treated BSPPs, the NRC culture medium was supplemented with 10% of Matrigel (Sigma) 2 days after photopolymerization. For all samples, culture media were renewed 3 times a week.

2.4. Fluorescent dye transport assay

On day 7 or day 21 of culture, BSPPs were incubated with fresh serum-free medium containing 15 μM of fluorescein diacetate (FDA, Sigma) for 5 min at 37 °C and were then washed with serum-free medium three times. BSPPs were visualized using an Olympus IX83-inverted microscope with a 10× objective or Leica DMi8 microscope equipped with 10× objective and images were taken every 10 min for 1 h. Temperature and CO_2 concentration were kept at 37 °C and 5%, respectively.

2.5. Fixation, immunofluorescent staining, and confocal microscopy of BSPP

To investigate the biliary epithelium formation *in vitro*, BSPPs cultured for a week in NRC culture medium supplemented with 10% of Matrigel for four days were fixed in 4% PFA in PBS for 15 min at room temperature, washed three times for 10 min in PBS and incubated for 1 h in blocking solution (5% normal goat serum (Cell Signaling Technology #5425), 0,3% Triton X-100 in PBS) at room temperature. The blocking was followed by overnight incubation with the primary antibodies (1% BSA, 0,3% Triton X-100 in PBS) at +4°. After three 10 min washings in PBS at room temperature, samples were incubated with secondary antibodies (1% BSA, 0,3% Triton X-100 in PBS) for 2 h at room temperature. Finally, samples were mounted using Aqua-Poly/Mount mounting medium and imaged using a confocal laser scanning microscope Zeiss LSM780 equipped with a 40× objective. Below is the list of used antibodies and dyes with the dilution ratios relative to stock concentrations

recommended by the manufacturers:

- anti-Acetyl-α-Tubulin (Cell Signaling Technology #5335) – 1:800;
- anti-ZO-1 (Invitrogen #33–9100) – 1:100;
- goat anti-Mouse IgG (Cy3) (Abcam #ab97035) – 1:200;
- goat anti-Rabbit IgG (Alexa Fluor 488) (Thermo Fisher Scientific #A-11034) – 1:200;
- phalloidin (Alexa Fluor 647) (Thermo Fisher Scientific #A22287) – 1:200;
- DAPI (Roche #10 236 276 001) – 4 μg/ml

2.6. Time-lapse image acquisition of BSPPs

Time-lapse microscopy was performed at 37 °C and 5% of CO_2, with images taken at 30-min intervals using an Olympus IX83-inverted microscope or a Leica DMi8 microscope equipped with a 10× objective.

2.7. FRAP-assays

FRAP-assays were performed using a confocal microscope ZEISS LSM 780 equipped with objective W Plan-Apochromat 20×/1.0 DIC M27. Three laser wavelengths were used simultaneously for bleaching at maximum intensity: 405 nm, 458 nm, and 488 nm. The bleaching of the 7 μm-wide line across the BSPP was performed in 64 passages of the laser beam.

2.8. Photopolymerizable hydrogel compositions

Before 3D stereolithography, various photopolymerizable hydrogel formulations were prepared: (i) C^{MA}/HA^{MA}/FG with 0.2% (w/v) C^{MA}, 0.3% (w/v) HA^{MA}, 0.14% (w/v) FG, and 1% (w/v) LAP (ii) C^{MA}/HA^{MA} with 0.2% (w/v) C^{MA}, 0.3% (w/v) HA^{MA}, and 1% (w/v) LAP (iii) C^{MA}/FG with 0.2% (w/v) C^{MA}, 0.14% (w/v) FG, and 1% (w/v) LAP (iv) HA^{MA}/FG with 0.3% (w/v) HA^{MA}, 0.14% (w/v) FG, and 1% (w/v) LAP (v) 0.2% (w/v) C^{MA} and 1% (w/v) LAP (vi) HA^{MA} with 0.3% (w/v) HA^{MA} and 1% (w/v) LAP (vii) FG with 0.14% (w/v) FG and 1% (w/v) LAP. Each previously described photopolymerizable hydrogel mix was gently mixed with NRCs at a cell concentration of 10^7 NRCs/mL and were photopolymerized with a 20 mJ/mm^2 dose. After being incubated in NRC medium for 48 h at 37 °C, the photopolymerized samples were cultured during 5 more days in NRC culture medium supplemented with 10% Matrigel.

2.9. Rheological analysis

Rheological features of photopolymerized hydrogels were measured by a Discovery HR 2 rheometer (TA Instruments) equipped with a parallel plate geometry (d = 25 mm). Two different photopolymerized hydrogel formulations were prepared: C^{MA}/HA^{MA}/FG (0.2% C^{MA}, 0.3% HA^{MA} 0.14% FG, 1% LAP) and C^{MA}/HA^{MA} (0.2% C^{MA}, 0.3% HA^{MA}, 1% LAP). Samples with a thickness of 100 μm and 25 mm in diameter were photopolymerized with a 20 mJ/mm^2 dose. After being incubated in NRC medium for 24 h at 37 °C, the photopolymerized samples were subjected to oscillatory measurements. In order to eliminate the environmental noise in data acquisition, the frequency sweeps were conducted at room temperature in the range of 0.1–10 Hz, and with a constant strain rate of 1%, considered to be in the linear viscoelastic range.

3. Results

3.1. Cholangiocytes embedded in 3D photopolymerized hydrogels of defined geometry can proliferate, migrate, and organize into branched tubular epithelial networks

Cholangiocyte cysts that form spontaneously in hydrogel environments consist of a central lumen surrounded by a monolayer of cells with apicobasal polarization [11,16,18,21,27]. When cultured in ECM derived from the decellularized liver [18], some cysts randomly adopt an elongated shape. However, their size and shape cannot be controlled, and the system is inappropriate for obtaining reproducible models of functional polarized intra-lobular bile ducts. In an attempt to guide cholangiocytes' self-organization towards tubes with predetermined geometry, we used DLP stereolithography to fabricate 3D hydrogel structures of various shapes encapsulating biliary epithelial cells (Fig. 1).

After surveying a panel of ECMs that have been shown to sustain (alone or in a mixture) the culture of epithelial cells [29], we focused on type I collagen, hyaluronic acid, and fibrinogen. In order to print the selected hydrogels using DLP stereolithography, we screened different formulations of methacrylated collagen (C^{MA}), methacrylated hyaluronic acid (HA^{MA}), and lithium phenyl-2,4,6 trimethyl-benzoyl phosphinate (LAP) – a cytocompatible photoinitiator [30], with or without fibrinogen (FG) (Fig. 2-Fig. S2).

C^{MA} is a photopolymerizable hydrogel produced from collagen that sustains good cell viability following encapsulation and retains natural cell-binding motifs [31,32]. HA^{MA} is also a photopolymerizable hydrogel derived from hyaluronic acid, the latter is found ubiquitously in native tissues and plays an important role in many cellular responses, such as cell signaling or cell proliferation[25–27]. FG is a component of the ECM that mediates cellular functions such as adhesion, spreading, proliferation, and migration of a variety of cell types, including fibroblasts, endothelial and epithelial cells. C^{MA} and HA^{MA} incorporation provides tunability of mechanical properties via variation of the UV dose and material concentration while still maintaining the essential features of the native biliary epithelial microenvironment [33,34]. The incorporation of FG changes the topology of the extracellular matrix in order to provide a surface for cell adhesion, migration, and matrix remodeling [35]. As illustrated in Fig. 2A, C^{MA} and HA^{MA} when used alone or in combination with FG could be photopolymerized with suspended cholangiocytes. However, C^{MA}, HA^{MA}/FG, and C^{MA}/FG hydrogels were rapidly degraded in the presence of living cells and thus did not offer enough stability to sustain the directed growth of any organized multicellular structure. This degradation was directly linked to the presence of living cells as the same hydrogel structures shown excellent stability over time in the absence of cells. In contrast, when all three components were mixed in a ratio of 0.2% (w/v):0.3% (w/v):0.14% (w/v) C^{MA}/-HA^{MA}/FG, photopolymerized hydrogel structures showed substantially higher stability over time and we observed migration and reorganization of the cholangiocytes within them. This reorganization however was not observed when fibrinogen was omitted in the 0.2% (w/v):0.3% (w/v) CMA/HA^{MA} mix.

Storage modulus (G′) and loss modulus (G″) were measured via frequency-dependent oscillatory rheological analysis to investigate the viscoelastic features of the fabricated hydrogels. As depicted in Fig. 2B and Fig. S2B, both C^{MA}/HA^{MA} and C^{MA}/HA^{MA}/FG formulations exhibited a classical hydrogel feature (G′ greater than G″), where G′ and G″ were kept nearly constant in the entire frequency range (0.1–10 Hz). These measurements also showed that the C^{MA}/HA^{MA}/FG mix photopolymerized at 20 mJ/mm^2 yielded a softer matrix compared to either C^{MA}/HA^{MA} photopolymerized with the same dose or C^{MA}/HA^{MA}/FG photopolymerized with a double dose. When NRCs were encapsulated in these three matrices, limited migration was observed for NRCs encapsulated in the slightly stiffer hydrogels (Fig. 2A, C^{MA}/HA^{MA} **day 7 and** Fig. S2A, **day 7**). These results suggest that it is not the presence per se of fibrinogen that is helping cell migration but rather a combination of its presence and a decrease in stiffness brought by the addition of this third component. . It is interesting to note that the storage modulus of the softer C^{MA}/HA^{MA}/FG photopolymerized hydrogel is in the same range of 50–800 Pa as the one measured by Lewis et al. for ECM derived from decellularized livers [18] in which cholangiocytes could reorganize *in vitro* into cystic and elongated structures. In parallel, by optimizing UV

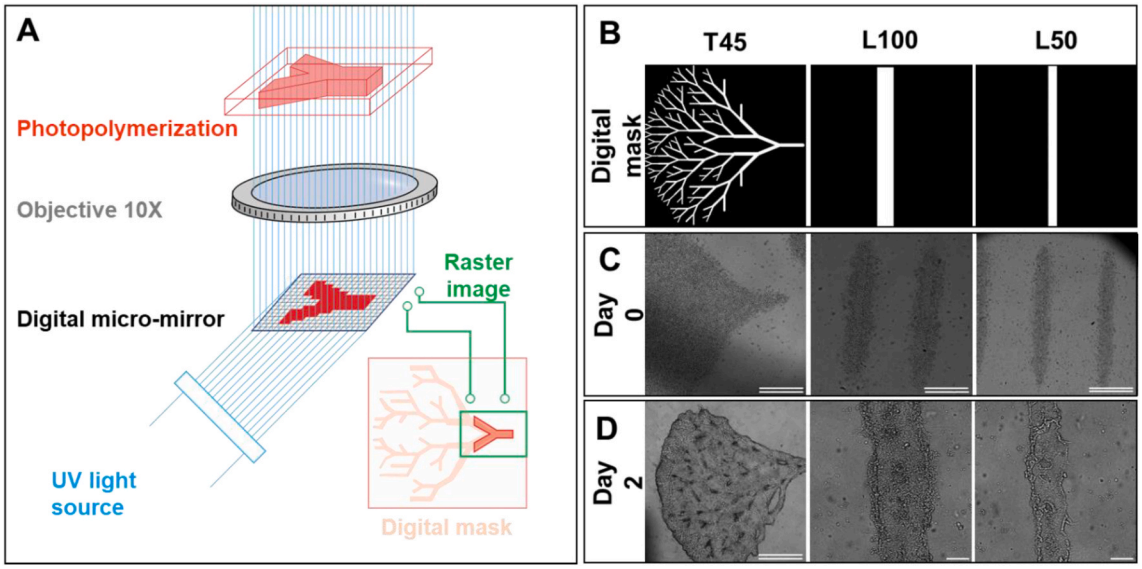

Fig. 1. Fabrication of BSPPs. (A) The scheme of DLP stereolithography. (B) Various digital patterns for BSPPs: a tree with 45° branching (T45), and lines of 100 μm (L100) and 50 μm (L50) width. (C, D) Cholangiocytes encapsulated into a correspondingly shaped photopolymerized hydrogel structures just after fabrication (C) and 2 days after the fabrication (D). Double-line scale bars are 1 mm and single line scale bars are 50 μm.

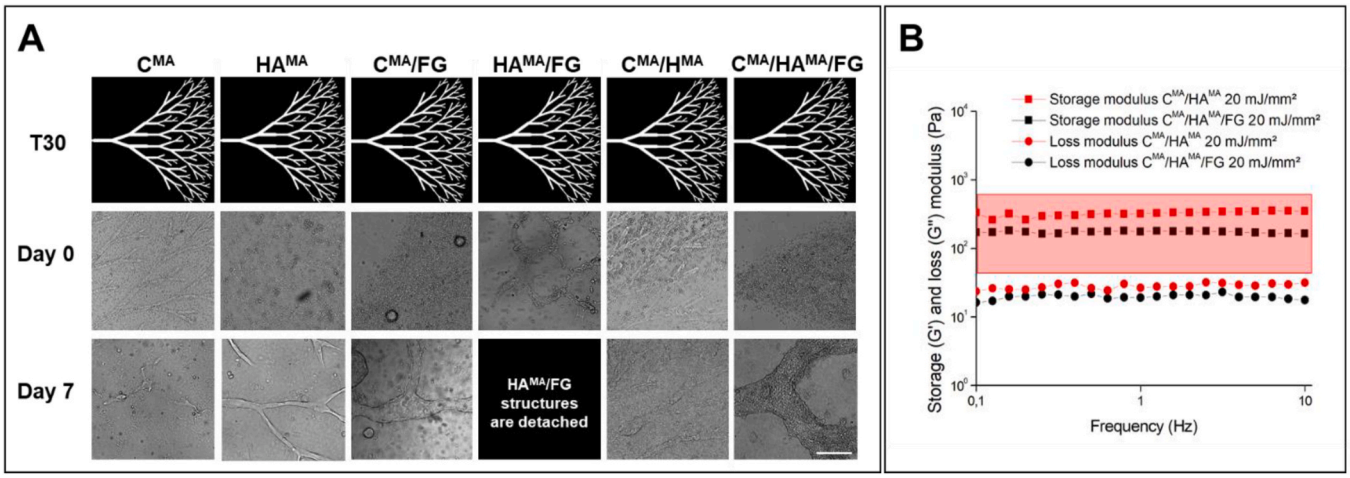

Fig. 2. *In vitro* characterization of various hydrogels for BSPPs. (A) Cholangiocytes encapsulated in various photopolymerized 30° tree hydrogels (T30) just after photopolymerization and 7 days after photopolymerization. It is worth noting that FG is not photopolymerizable using the LAP photoinitiator. Scale bar is 200 μm. (B) Rheological analysis of the photopolymerized hydrogels used to encapsulate cholangiocytes in comparison with the storage modulus range for optimal concentration of decellularized liver ECM enabling tubulogenesis according to Lewis et al. (red framed rectangle) [18]. (For interpretation of the references to colour in this figure legend, the reader is referred to the Web version of this article.)

doses and concentration of LAP, we confirmed that cells had good viability 4 h and 24 h after printing (Fig. S1).

We also explored various patterns of lines ranging from 10 to 500 μm in width and trees with branching angles of 30, 45, and 60° (Fig. 1 and Fig. S3). In all cases, we found that, just after photopolymerization, cells were trapped in an area larger than the one defined by the optical mask (Fig. 1C). This is most likely the result of light scattering, thereby inducing partial photopolymerization in adjacent regions and decreasing the expected resolution [36]. Nevertheless, after two days in culture, the structures had condensed (Fig. 1D) and the resulting structures were close in size to the original projected pattern, as if the cells had clustered together around the harder polymerized backbone.

3.2. Matrigel is a key component for obtaining stable BSPPs

In previous studies exploring the 3D culture of biliary epithelial cells [18,21], type I collagen alone was insufficient to sustain the formation of any organized structure and Matrigel was required to form polarized structures with lumens [16,18,21]. Furthermore, the known association between biliary epithelial cells and basal lamina during bile duct morphogenesis led to the hypothesis that the basal lamina components are necessary to mimic the *in vivo* environment of developing bile ducts [21]. In order to evaluate this hypothesis, we supplemented the culture media, 2 days after photopolymerization, with 10% Matrigel whose composition closely mimics the components of the basal lamina, including especially laminin-1 which is crucial for epithelial polarization of mature cholangiocytes [21]. One week after photopolymerization, biliary epithelial cells in the samples without Matrigel failed to maintain organized structures (Fig. 3, **left panel**), whereas, in the presence of Matrigel, stable tubular and branched structures were maintained. The geometry of these structures correlated with the shapes on the original optical masks, with lengths up to 2 mm and widths

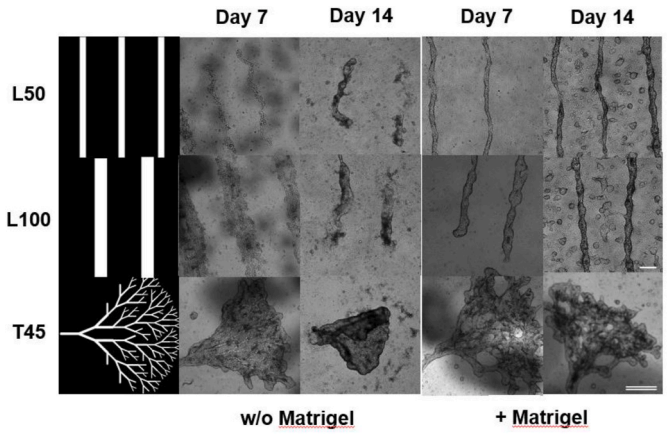

Fig. 3. BSPP formation over time. Two days after fabrication and culture in cholangiocyte medium, BSPPs were divided into 2 groups and cultured respectively with and without Matrigel. Cholangiocytes were encapsulated either in 50 μm photopolymerized lines (L50), 100 μm photopolymerized lines (L100), and 45° photopolymerized trees (T45) and imaged after 7 and 14 days respectively. Single line scale bar is 200 μm (50–100 μm lines) and double-line scale bar is 1 mm (45° trees).

ranging from 10 μm up to 100 μm for linear tubes (Fig. 3, **right panel and** Fig. S3, **day 7**). Cells trapped within the proximal photopolymerization zones due to light scattering were also able to actively migrate and significantly remold the photopolymerized hydrogel structures between days 2–7. This resulted in modification of feature shapes and sizes compared to the ones dictated by original optical masks, especially when considering complex geometries such as the smallest branches of trees (<20 μm). Seven days after photopolymerization, of which 5 days in culture media supplemented with Matrigel, we observed that the smallest branches of the 30° and 45° trees could not be resolved using our stereolithographic technique while the ones of 60° trees were often resolved (Fig. S3, day 7) and had cystic-shaped extremities.

Two weeks after fabrication, in the samples without Matrigel, BSPPs were partially degraded and detached from the glass substrate (Fig. 3 left panel, Fig. S4) whereas, in the presence of Matrigel, BSPPs could be maintained up to 21 days (Fig. 3 right panel, Fig. S3, day 14 and day 21, and Fig. S5).

These results suggest that DLP stereolithographic bioprinting can efficiently create a 3D ECM scaffold that guides proliferation, migration, and rearrangement of cholangiocytes when cultured in a medium supplemented with Matrigel and that the resulting structures can be maintained for at least 21 days after photopolymerization.

3.3. The obtained BSPPs have a monolayer wall and actively transport fluorescein from the cytoplasm into the lumen

Knowing that biliary epithelial cells spontaneously form cysts with a monolayer wall when cultured in natural or synthetic hydrogels [11,16], we sought to investigate whether the BSPPs were forming lumens and whether these constructs could elicit the basic functions of biliary epithelium.

After 7 days of culture, of which 5 days in medium supplemented with Matrigel, BSPPs were fixed, stained, and imaged using a laser scanning confocal microscope. Staining with phalloidin, anti-ZO1 antibodies, and DAPI revealed that the cholangiocytes in BSPPs are organized in a monolayer around a central lumen. These tubes could span hundreds of microns without any visible breaks in the walls. The diameter of the lumen was close to the size of the initial photopolymerized hydrogel structure as it can be seen in Fig. 4: a tube with a 20–40 μm lumen (Fig. 4A) was formed on a 50 μm photopolymerized line, while the tube with the 10–15 μm lumen (Fig. 4B) resulted from a 20 μm photopolymerized line. Moreover, F-actin distribution was characteristic of epithelial cells with dense bands along cell-cell borders. Cholangiocytes formed tight junctions as shown by ZO-1 staining suggesting the formation of an intact epithelial barrier.

We further characterized the polarization of the cholangiocytes in BSPP tubes by staining them for acetylated alpha-tubulin - a component of the primary cilia. A number of cells had developed primary cilia and these were all facing the lumen (Fig. 4C).

Functional characterization of BSPP tubes was performed using the fluorescein diacetate (FDA) assay. FDA is a non-fluorescent molecule, which living cells hydrolyze to form fluorescent fluorescein in their cytoplasm. Cholangiocytes, unlike most non-epithelial cells, can further secrete fluorescein through specific MRP2 [37–40] transporters located on their apical membranes [41–43]. As shown in Fig. 5, our BSPPs actively transported fluorescein into the lumen, in both linear BSPPs of different diameters and branched BSPPs. The same result was obtained

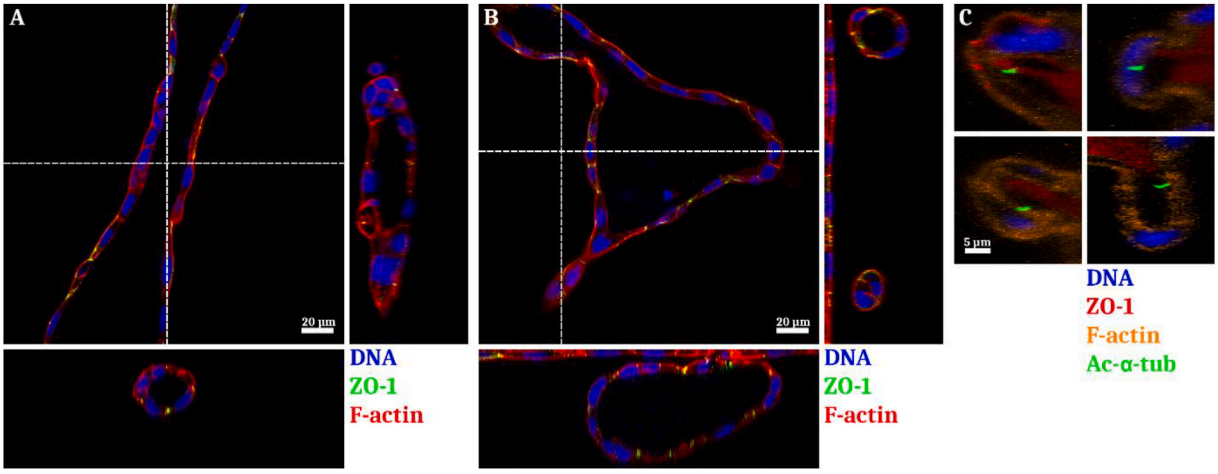

Fig. 4. Confocal imaging of BSPPs after 7 days of culture in media supplemented with Matrigel for 5 days. NRC form single-layer tubular structures from an (A) 50 μm photopolymerized line and (B) tree-like branching structure. Staining for F-actin (phalloidin), tight junctions (anti-ZO-1 immunostaining), and DNA (DAPI). (C) Additional staining for acetylated α-tubulin reveals cilia facing the lumen of our tubular structures and formed by NRCs (orange – F-actin; red – ZO-1; green – acetylated α-tubulin; blue – DNA). Dashed lines indicate where the reconstructed Z-slices are located. Confocal imaging using Zeiss LSM 780 equipped with a 40× objective. Scale bar – 20 μm for A and B, 5 μm for C. (For interpretation of the references to colour in this figure legend, the reader is referred to the Web version of this article.)

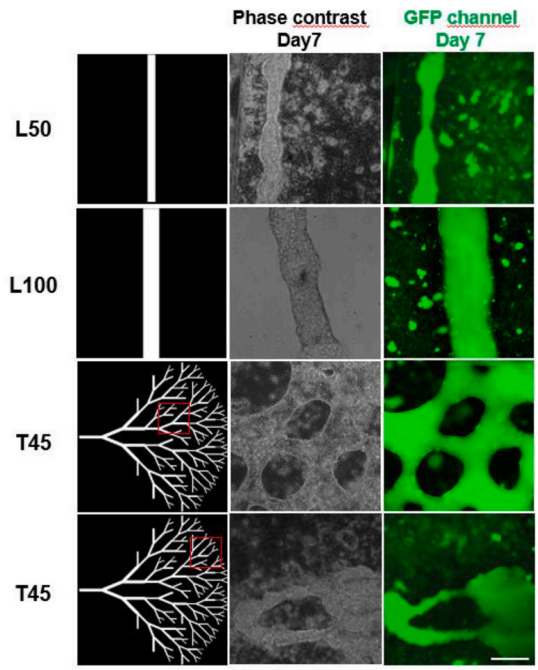

Fig. 5. Functional characterization of BSPPs with a FDA assay. 7-day-old BSPPs were incubated with FDA and imaged with fluorescence microscope to evaluate the transport of fluorescein inside the lumen. Scale bar is 100 μm.

with Rhodamine 123 – a fluorescent compound secreted by MDR-1 – another anion transporter localized on the apical membrane (Fig. S7). To confirm that the fluorescent signal is coming from fluorescent molecules transported inside the luminal space and not only from the cell monolayer, we also performed a series of confocal FRAP-tests (Fig. 6) with some of the FDA-treated samples. We quenched a 7 μm-wide line across the tube and thus bleached the signal coming from the cells and the lumen. Immediately after, we observed unperturbed rapid diffusion of fluorescein inside the BSPP lumen, restoring a homogeneous signal within seconds, whereas the bleached cells remained dark. In both these last sets of experiments, the fluorescent signal appeared homogeneous throughout the branched tubular structure, confirming a closed and continuous luminal space with no gaps in the walls over hundreds of microns.

Taken together, these results demonstrate that we are able to produce geometrically controlled biliary tubes possessing structural and functional properties of intrahepatic bile ducts using DLP stereolithography to encapsulate cholangiocytes in soft hydrogels.

4. Discussion and conclusions

Cholangiocytes, like many epithelial cells, are known to spontaneously form cysts, sometimes adopting an elongated tubular structure [11,18]. However, the absence of control over their size and shape prevents the development of reproducible models of functional polarized intra-lobular bile ducts. In this work, we demonstrate that the control over the initial geometry of a hydrogel by DLP stereolithography can allow the guided self-organization and polarization of embedded cholangiocytes into biliary tubes with predefined geometries including linear tubes with diameters found in the intrahepatic region of the biliary tree and, most remarkably, branched networks in tree-like configurations. Hence, this work stands as a striking illustration of how engineering techniques, in particular micropatterning as well as bioprinting, can help unleash the full potential of cellular self-organization into reproducibly building functional tissues and mini-organs with higher fidelity and robustness as discussed previously in our review [44] and illustrated here, as well as in our recent paper [45].

The composition of the gel was a critical parameter and the conjunction of all three types of matrices proved to be necessary to sustain self-organization. The precise role of each component has yet to be elucidated, although hypotheses can be made based on what is already known about these natural extracellular matrix polymers. Type I collagen is by far the most abundant protein in all vertebrates. It autoassembles into heterofibrils with either type III or type V collagen. Heterofibrils are the structural and mechanical scaffold of most parenchymal tissues such as the lung, kidney, liver, muscle, or spleen. Type I collagen is in particular present in normal livers in the blood vessel walls and the wall of biliary ducts of the portal tracts [46]. C^{MA} alone was rapidly degraded in the presence of cells in our initial experiments and the addition of HA^{MA} improved the durability of the photopolymerized hydrogel. Indeed, hyaluronic acid is known to improve the mechanical properties of constructs in tissue engineering applications. It is also known to improve cell migration of cornea epithelial cells [47] and both these properties could play a role in promoting efficient and stable tissue self-organization in this study. FG in turn plays a critical role in inflammation, wound healing, and angiogenesis. Blood cells, endothelial cells, and cells of other types interact with FG while spreading into the extravascular space. FG has been implicated in particular as a substratum for epithelial cell migration during wound repair [48–50]. Our results with BSPPs show that the addition of FG was indeed essential for cholangiocyte tube formation as shown in Fig. 2 where NRC structures following the initial photopattern are seen after 7 days with the C^{MA}, HA^{MA}, and FG mix but not with C^{MA} or HA^{MA} alone. However, the degree of crosslinking, affecting the stiffness of the resulting hydrogel, was also a paramount parameter since its increase for the same triad of hydrogels prevented tube formation.

As illustrated by Fig. 3 and by the supplementary movies S8 and S9, tubes form by proliferation and collective migration of cholangiocytes which seem to engulf the 3D structures, working their way between the

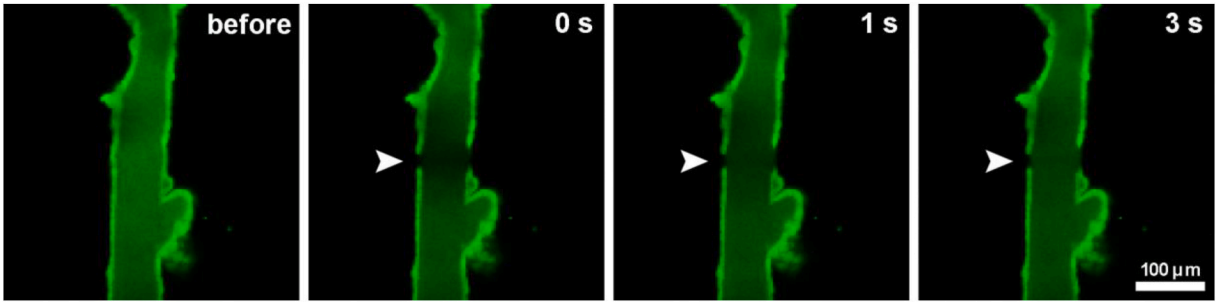

Fig. 6. Fluorescein diffusion in BSPPs in FRAP-assays. BSPP samples were subjected to a FDA assay and imaged used a FRAP setup. A thin line (~7 μm-wide) perpendicular to the long axis of the BSPP was bleached using 405 nm, 458 nm and 488 nm lasers (designated with arrowheads in the figure). Confocal imaging using a Zeiss LSM 780 equipped with a 20× objective was carried out at the indicated time points to follow fluorescein diffusion in the BSPP.

glass and the hydrogel and eventually closing the tube when the two edges of the cell monolayers meet over the hydrogel. In some movies (in particular movies S9B and S9D) a "zipper" type of closing of these two sheets can be observed. These tubes form within a few days and Matrigel, added two days after photopolymerization, plays a critical role in the stability of these tubes over time: at early time points up to the third or fourth day after photopolymerization, depending on the initial geometry of the construct, functional tubes can be observed without Matrigel, but these are unstable and collapse rapidly (movies S8). In the presence of Matrigel, tubes are stable, functional, and can be maintained for up to 21 days. At later stages, transport assays show that these tubes dissipated the fluorescent dye very quickly from the central lumen, pointing to defects in the overall integrity of the tube after 21 days (Fig. S6). The process whereby Matrigel stabilizes these tubes has yet to be elucidated. In our conditions, the concentration of Matrigel is insufficient for actual gel formation, which means that its role is not one of physical support. We hypothesize that a component of the ECM, most probably laminin, is reinforcing the polarization of the tube by offering a basal signal to the outside of the tube.

It is interesting to note that the collapse process observed without Matrigel initiates from a central point and forms circular expanding structures that break up the initially condensed tubular structure. We hypothesize that the polarity of cells is randomly distributed in these constructs without the basal signaling brought by the laminin-containing Matrigel. It then appears that an avalanche effect leads to a collective collapse initiating from a central node. In itself, this mechanism would be interesting to elucidate further.

Finally, from an application standpoint, the microfabrication process described here provides a means to obtain functional, robust, and reproducible *in vitro* tissue models which are much needed for a wide range of screening applications. However, in terms of relevance for pharmacology and clinical applications, this model will need to be reproduced using cells of human origin once the reliable sources of human cholangiocytes become available. Nonetheless, our BSPPs, as well as those recently published with our collaborators using a micropatterning technique [47], are the first *in vitro* models of intrahepatic bile tubules which should prove invaluable to test receptor-mediated transport functions, drug transport and help elucidate precise mechanisms and gene functions involved in the function of the biliary tree. Indeed, the tree-like design of our biliary structures represents a planar mimic of the intrahepatic biliary network that collects bile into bigger bile ducts. We can then envision that the secreted bile in the BSPP could be collected and analyzed in an integrated microfluidic circuit, for example by fabricating the soft hydrogel structure at the extremity of a silica microcapillary (with a diameter in the range of 100 μm) immobilized on the glass coverslip and subsequently allowing the cholangiocytes to self-organize into tubes, thus connecting a "soft" microfluidic network to the external "hard" microfluidic circuit. This would allow the study of the initiation of any spontaneous flow from the microfabricated biliary network and the recovery of bile, although the addition of hepatocytes to the model would then be essential to recreate the full transport cascade between hepatocytes, bile canaliculi, and cholangiocyte biliary tubules. Interestingly, in contrast to what is obtained inside bulk porous hydrogels, the tubes obtained in this setup offer full access to the outside of the tube, allowing the introduction of other cell types, such as hepatocytes and endothelial cells, at any stage of BSPP maturation. This was illustrated by our collaborators who found that in the absence of hydrogel support such as the one described here, the preseeding of endothelial cells on 2D tree micropatterns was critical to obtain stable closed cholangiocyte tubes with continuous lumens [45]. We now envisage the addition of hepatocytes or hepatoblasts to our model, either preorganized as spheroids, or as a cell sheet [51] that we would stack over the planar biliary tree. We aim to elucidate further the spontaneous reorganization of these hepatocyte/blast structures over the biliary network and study any interaction/reorganization of the bile canaliculi structures with the biliary network. The planar organization of our model and its localization in close proximity to a glass coverslip are additional advantages for conducting such studies using confocal microscopy as illustrated here.

These co-culture experiments remain however extremely challenging, notably in selecting the most promising cells, their degree of differentiation, their origin, the proper ratio between various cell types, the compatible cell co-culture media to support cell survival and migration, and in controlling proliferation. As all tissues are composed of multiple cell types, these hurdles are present in all tissue engineering endeavors and will need to be addressed as the research field moves towards more and more complex *in vitro* human models.

Funding and acknowledgments

This work received the financial support of the iLite RHU program (grant ANR ANR-16-RHUS-0005).

We thank Didier Letourneur and Isabelle Bataille (INSERM U1148, Univ Paris 13) for access to their rheology equipment. We also thank Latifa Bouzhir for her assistance with NRC culture. We thank the Technological Core Facility of the Institut de Recherche Saint-Louis, Université Paris-Diderot for continued support in multimodal microscopy.

We finally thank Benoit Vianay from the CytoMorphoLab (INSERM, CEA, U976) for his technical assistance with the DLP stereolithography setup.

Author contributions

E.M-A. D.A. F.C. and A.F. conceived and designed the experiments; E. M-A. D.A., E.G., A.M., and W.F. performed the experimental work and contributed to the manipulation of materials, reagents, and analysis tools; E.M-A. D.A. W.F., P. D-W, F.C., J.L, and A.F. analyzed the data and wrote the manuscript. All authors read and approved the final manuscript.

Declaration of competing interest

The authors declare that they have no known competing financial interests or personal relationships that could have appeared to influence the work reported in this paper.

Appendix A. Supplementary data

Supplementary data to this article can be found online at https://doi.org/10.1016/j.biomaterials.2021.121207.

References

[1] C.C. Bell, et al., Comparison of hepatic 2D sandwich cultures and 3D spheroids for long-term toxicity applications: a multicenter study, Toxicol. Sci. 162 (2) (2018), https://doi.org/10.1093/toxsci/kfx289. Art. no 2, avr.

[2] F. Meier, et al., Hepatic differentiation of human iPSCs in different 3D models: a comparative study, Int. J. Mol. Med. 40 (6) (2017), https://doi.org/10.3892/ijmm.2017.3190. Art. no 6, déc.

[3] K. Sakabe, T. Takebe, et A. Asai, Organoid medicine in hepatology, Clin. Liver Dis. 15 (1) (2020) 3–8, https://doi.org/10.1002/cld.855.

[4] G.H. Underhill, et S.R. Khetani, Bioengineered liver models for drug testing and cell differentiation studies, Cell. Mol. Gastroenterol. Hepatol. 5 (3) (2018) 426–439, https://doi.org/10.1016/j.jcmgh.2017.11.012, e1, janv.

[5] G.H. Underhill, et S.R. Khetani, Advances in engineered human liver platforms for drug metabolism studies, Drug Metab. Dispos. Biol. Fate Chem. 46 (11) (2018) 1626–1637, https://doi.org/10.1124/dmd.118.083295.

[6] H. Hu, et al., Long-Term expansion of functional mouse and human hepatocytes as 3D organoids, Cell 175 (6) (2018) 1591–1606, https://doi.org/10.1016/j.cell.2018.11.013, e19, nov.

[7] T. Takebe, et al., Massive and reproducible production of liver buds entirely from human pluripotent stem cells, Cell Rep. 21 (10) (2017), https://doi.org/10.1016/j.celrep.2017.11.005. Art. no 10, déc.

[8] J.H. Tabibian, et al., Randomised clinical trial: vancomycin or metronidazole in patients with primary sclerosing cholangitis - a pilot study, Aliment. Pharmacol. Ther. 37 (6) (2013), https://doi.org/10.1111/apt.12232. Art. no 6, mars.

[9] Y. Nakanuma, K. Tsuneyama, et K. Harada, Pathology and pathogenesis of intrahepatic bile duct loss, J. Hepatobiliary. Pancreat. Surg. 8 (4) (2001) 303–315, https://doi.org/10.1007/s005340170002.

[10] O.C. Tysoe, et al., Isolation and propagation of primary human cholangiocyte organoids for the generation of bioengineered biliary tissue, Nat. Protoc. 14 (6) (2019), https://doi.org/10.1038/s41596-019-0168-0. Art. no 6, juin.

[11] C. Chen, et al., Bioengineered bile ducts recapitulate key cholangiocyte functions, Biofabrication 10 (3) (2018), https://doi.org/10.1088/1758-5090/aac8fd. Art. no 3, juin.

[12] P.M. Baptista, M.M. Siddiqui, G. Lozier, S.R. Rodriguez, A. Atala, et S. Soker, The use of whole organ decellularization for the generation of a vascularized liver organoid, Hepatology 53 (2) (2011), https://doi.org/10.1002/hep.24067. Art. no 2, févr.

[13] W. Hassanein, et al., Recellularization via the bile duct supports functional allogenic and xenogenic cell growth on a decellularized rat liver scaffold, Organogenesis 13 (1) (2017), https://doi.org/10.1080/15476278.2016.1276146. Art. no 1, 02.

[14] T. Katsuda, N. Kojima, T. Ochiya, et Y. Sakai, Biliary epithelial cells play an essential role in the reconstruction of hepatic tissue with a functional bile ductular network, Tissue Eng. 19 (no 21–22) (2013), https://doi.org/10.1089/ten.TEA.2013.0021. Art. no 21-22, nov.

[15] M.K. Auth, et al., Morphogenesis of primary human biliary epithelial cells: induction in high-density culture or by coculture with autologous human hepatocytes, Hepatol. Baltim. Md 33 (3) (2001), https://doi.org/10.1053/jhep.2001.22703. Art. no 3, mars.

[16] A. Funfak, L. Bouzhir, E. Gontran, N. Minier, P. Dupuis-Williams, et S. Gobaa, Biophysical control of bile duct epithelial morphogenesis in natural and synthetic scaffolds, Front. Bioeng. Biotechnol. 7 (2019) 417, https://doi.org/10.3389/fbioe.2019.00417.

[17] F. Sampaziotis, et al., Cholangiocyte organoids can repair bile ducts after transplantation in the human liver, Science 371 (6531) (2021) 839–846, https://doi.org/10.1126/science.aaz6964, févr.

[18] P.L. Lewis, et al., Complex bile duct network formation within liver decellularized extracellular matrix hydrogels, Sci. Rep. 8 (1) (2018), https://doi.org/10.1038/s41598-018-30433-6. Art. no 1, déc.

[19] L. Tian, A. Deshmukh, Z. Ye, et Y.-Y. Jang, Efficient and controlled generation of 2D and 3D bile duct tissue from human pluripotent stem cell-derived spheroids, Stem Cell Rev. 12 (4) (2016), https://doi.org/10.1007/s12015-016-9657-5. Art. no 4, août.

[20] M. K. Auth et al., « Morphogenesis of primary human biliary epithelial cells: induction in high-density culture or by coculture with autologous human hepatocytes », Hepatol. Baltim. Md, vol. 33, n° 3, p. 519-529, mars 2001, doi: 10.1053/jhep.2001.22703.

[21] N. Tanimizu, A. Miyajima, et K.E. Mostov, Liver progenitor cells develop cholangiocyte-type epithelial polarity in three-dimensional culture, Mol. Biol. Cell 18 (4) (2007) 1472–1479, https://doi.org/10.1091/mbc.E06-09-0848, avr.

[22] M.K.H. Auth, et al., Morphogenesis of primary human biliary epithelial cells: induction in high-density culture or by coculture with autologous human hepatocytes, Hepatology 33 (3) (2001), https://doi.org/10.1053/jhep.2001.22703. Art. no 3.

[23] W. Hashimoto, R. Sudo, K. Fukasawa, M. Ikeda, T. Mitaka, et K. Tanishita, Ductular network formation by rat biliary epithelial cells in the dynamical culture with collagen gel and dimethylsulfoxide stimulation, Am. J. Pathol. 173 (2) (2008) 494–506, https://doi.org/10.2353/ajpath.2008.071024, août.

[24] Y. Ishida, et al., Ductular morphogenesis and functional polarization of normal human biliary epithelial cells in three-dimensional culture, J. Hepatol. 35 (1) (2001) 2–9, https://doi.org/10.1016/S0168-8278(01)00078-2, juill.

[25] J.A. Brassard, M. Nikolaev, T. Hübscher, M. Hofer, et M.P. Lutolf, Recapitulating macro-scale tissue self-organization through organoid bioprinting, Nat. Mater. 20 (1) (2021), https://doi.org/10.1038/s41563-020-00803-5. Art. no 1, janv.

[26] X. Ma, et al., Deterministically patterned biomimetic human iPSC-derived hepatic model via rapid 3D bioprinting, Proc. Natl. Acad. Sci. Unit. States Am. 113 (8) (2016), https://doi.org/10.1073/pnas.1524510113. Art. no 8, févr.

[27] B. Vroman, et N.F. LaRusso, Development and characterization of polarized primary cultures of rat intrahepatic bile duct epithelial cells, Lab. Investig. J. Tech. Methods Pathol. 74 (1) (1996) 303–313, janv.

[28] P.C. de Groen, B. Vroman, K. Laakso, et N.F. LaRusso, Characterization and growth regulation of a rat intrahepatic bile duct epithelial cell line under hormonally defined, serum-free conditions, In Vitro Cell. Dev. Biol. Anim. 34 (9) (1998) 704–710, https://doi.org/10.1007/s11626-998-0066-1, oct.

[29] R.I. Freshney, Introduction, in: Culture of Epithelial Cells, John Wiley & Sons, Ltd, 2002, pp. 1–30, https://doi.org/10.1002/0471221201.ch1.

[30] B.D. Fairbanks, M.P. Schwartz, C.N. Bowman, et K.S. Anseth, Photoinitiated polymerization of PEG-diacrylate with lithium phenyl-2,4,6-trimethylbenzoylphosphinate: polymerization rate and cytocompatibility, Biomaterials 30 (35) (2009) 6702–6707, https://doi.org/10.1016/j.biomaterials.2009.08.055, déc.

[31] I.D. Gaudet, et D.I. Shreiber, Characterization of methacrylated type-I collagen as a dynamic, photoactive hydrogel, Biointerphases 7 (1–4) (2012) 25, https://doi.org/10.1007/s13758-012-0025-y, déc.

[32] E.E. Antoine, P.P. Vlachos, et M.N. Rylander, Review of collagen I hydrogels for bioengineered tissue microenvironments: characterization of mechanics, structure, and transport, Tissue Eng. B Rev. 20 (6) (2014) 683–696, https://doi.org/10.1089/ten.teb.2014.0086, déc.

[33] D. Fan, U. Staufer, et A. Accardo, Engineered 3D polymer and hydrogel microenvironments for cell culture applications, Bioengineering 6 (4) (2019), https://doi.org/10.3390/bioengineering6040113. Art. no 4, déc.

[34] B. S. Spearman, N. K. Agrawal, A. Rubiano, C. S. Simmons, S. Mobini, et C. E. Schmidt, « Tunable methacrylated hyaluronic acid-based hydrogels as scaffolds for soft tissue engineering applications », J. Biomed. Mater. Res. A, vol. 108, n° 2, p. 279-291, févr. 2020, doi: 10.1002/jbm.a.36814.

[35] Jennifer Shepherd, Daniel Bax, Serena Best, et Ruth Cameron, Collagen-fibrinogen lyophilised scaffolds for soft tissue regeneration, Materials 10 (6) (2017) 568, https://doi.org/10.3390/ma10060568, mai.

[36] S. You, P. Wang, J. Schimelman, H.H. Hwang, et S. Chen, High-fidelity 3D printing using flashing photopolymerization, Addit. Manuf. 30 (2019) 100834, https://doi.org/10.1016/j.addma.2019.100834, déc.

[37] P. Bravo, V. Bender, et D. Cassio, Efficient in Vitro vectorial transport of a fluorescent conjugated bile acid analogue by polarized hepatic hybrid WIF-B and WIF-B9 cells, Hepatology 27 (2) (1998) 576–583, https://doi.org/10.1002/hep.510270236.

[38] M.M. Malinen, et al., Differentiation of liver progenitor cell line to functional organotypic cultures in 3D nanofibrillar cellulose and hyaluronan-gelatin hydrogels, Biomaterials 35 (19) (2014) 5110–5121, https://doi.org/10.1016/j.biomaterials.2014.03.020, juin.

[39] U. Beuers, et al., Tauroursodeoxycholic acid inserts the apical conjugate export pump, Mrp2, into canalicular membranes and stimulates organic anion secretion by protein kinase C–dependent mechanisms in cholestatic rat liver, Hepatology 33 (5) (2001) 1206–1216, https://doi.org/10.1053/jhep.2001.24034.

[40] C.A. Barth, et L.R. Schwarz, Transcellular transport of fluorescein in hepatocyte monolayers: evidence for functional polarity of cells in culture, Proc. Natl. Acad. Sci. Unit. States Am. 79 (16) (1982) 4985–4987, https://doi.org/10.1073/pnas.79.16.4985, août.

[41] S. Glaser, et al., Differential transcriptional characteristics of small and large biliary epithelial cells derived from small and large bile ducts, Am. J. Physiol. Gastrointest. Liver Physiol. 299 (3) (2010) G769-G777, https://doi.org/10.1152/ajpgi.00237.2010, juin.

[42] D. Rost, J. König, G. Weiss, E. Klar, W. Stremmel, et D. Keppler, Expression and localization of the multidrug resistance proteins MRP2 and MRP3 in human gallbladder epithelia, Gastroenterology 121 (5) (2001) 1203–1208, https://doi.org/10.1053/gast.2001.28648, nov.

[43] E. Luce, et A. Dubart-Kupperschmitt, J.R. Spence, Chapter 4 - pluripotent stem cell-derived cholangiocytes and cholangiocyte organoids, in: Methods in Cell Biology, vol. 159, Academic Press, 2020, pp. 69–93, https://doi.org/10.1016/bs.mcb.2020.03.011.

[44] J. Laurent, et al., Convergence of microengineering and cellular self-organization towards functional tissue manufacturing, Nat. Biomed. Eng. 1 (12) (2017), https://doi.org/10.1038/s41551-017-0166-x. Art. no 12, déc.

[45] E. Gontran et al., « Self-organogenesis from 2D micropatterns to 3D biomimetic biliary trees », Bioeng. Basel Switz., vol. 8, n° 8, p. 112, août 2021, doi: 10.3390/bioengineering8080112.

[46] B. Voss, J. Rauterberg, S. Allam, et G. Pott, Distribution of collagen type I and type III and of two collagenous components of basement membranes in the human liver, Pathol. Res. Pract. 170 (1) (1980) 50–60, https://doi.org/10.1016/S0344-0338(80)80155-5, déc.

[47] J.a.P. Gomes, R. Amankwah, A. Powell-Richards, et H.S. Dua, Sodium hyaluronate (hyaluronic acid) promotes migration of human corneal epithelial cells in vitro, Br. J. Ophthalmol. 88 (6) (2004) 821–825, https://doi.org/10.1136/bjo.2003.027573, juin.

[48] D.J. Donaldson, J.T. Mahan, D. Amrani, et J. Hawiger, Fibrinogen-mediated epidermal cell migration: structural correlates for fibrinogen function, J. Cell Sci. 94 (Pt 1) (1989) 101–108, sept.

[49] R. Clark, et H. Peter, The Molecular and Cellular Biology of Wound Repair, Springer US, 1988, https://doi.org/10.1007/978-1-4615-1795-5.

[50] G. Guadiz, L.A. Sporn, R.A. Goss, S.O. Lawrence, V.J. Marder, et P.J. Simpson-Haidaris, Polarized secretion of fibrinogen by lung epithelial cells, Am. J. Respir. Cell Mol. Biol. 17 (1) (1997) 60–69, https://doi.org/10.1165/ajrcmb.17.1.2730, juill.

[51] K. Matsuura, R. Utoh, K. Nagase, et T. Okano, Cell sheet approach for tissue engineering and regenerative medicine, J. Control. Release Off. J. Control. Release Soc. 190 (2014) 228–239, https://doi.org/10.1016/j.jconrel.2014.05.024, sept.